

Accepted Manuscript

In vivo dynamics of the internal fibrous structure in smooth adhesive pads of insects

Jan-Henning Dirks, Minghe Li, Alexandre Kabla, Walter Federle

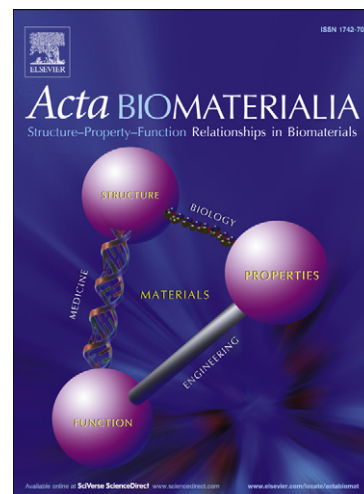
PII: S1742-7061(12)00155-9
DOI: [10.1016/j.actbio.2012.04.008](https://doi.org/10.1016/j.actbio.2012.04.008)
Reference: ACTBIO 2163

To appear in: *Acta Biomaterialia*

Received Date: 4 January 2012
Revised Date: 20 March 2012
Accepted Date: 3 April 2012

Please cite this article as: Dirks, J-H., Li, M., Kabla, A., Federle, W., *In vivo* dynamics of the internal fibrous structure in smooth adhesive pads of insects, *Acta Biomaterialia* (2012), doi: [10.1016/j.actbio.2012.04.008](https://doi.org/10.1016/j.actbio.2012.04.008)

This is a PDF file of an unedited manuscript that has been accepted for publication. As a service to our customers we are providing this early version of the manuscript. The manuscript will undergo copyediting, typesetting, and review of the resulting proof before it is published in its final form. Please note that during the production process errors may be discovered which could affect the content, and all legal disclaimers that apply to the journal pertain.



1 ***In vivo* dynamics of the internal fibrous structure in**
2 **smooth adhesive pads of insects**

3

4 Jan-Henning Dirks ^{*1,4}, Minghe Li ², Alexandre Kabla ³ and Walter Federle ⁴

5 ¹ Present address: Department of Mechanical and Manufacturing Engineering, Trinity College Dublin, Dublin 2, Ireland; ²
6 Department of Control Science, Tongji University, Shanghai, China; ³ Department of Engineering, University of Cambridge,
7 Cambridge CB2 1PZ, United Kingdom; ⁴ Department of Zoology, University of Cambridge, Cambridge CB2 3EJ, United
8 Kingdom

9 * Corresponding author: Jan-Henning Dirks – jan-henning.dirks@web.de; +353 (1) 896 1464

10 **Abstract**

11 Many insects with smooth adhesive pads can rapidly enlarge their contact area by
12 centripetal pulls on the legs, allowing them to cope with sudden mechanical
13 perturbations such as gusts of wind or raindrops. The short time scale of this reaction
14 excludes any neuromuscular control; it is thus more likely to be caused by mechanical
15 properties of the pad's specialised cuticle. This soft cuticle contains numerous
16 branched fibrils oriented almost perpendicularly to the surface. Assuming a fixed
17 volume of the water-filled cuticle, we hypothesized that pulls could decrease the fibril
18 angle, thereby helping the contact area to expand laterally and longitudinally.

19 Three-dimensional fluorescence microscopy on the cuticle of smooth stick insect pads
20 confirmed that pulls significantly decreased the fibril angle. The fibril angle variation
21 appeared insufficient to explain the observed increase in contact area. Direct strain
22 measurements in the contact zone demonstrate that pulls not only expand the cuticle
23 laterally (indicating a negative Poisson's ratio of the pad's cuticle), but also add new
24 contact area at the pad's perimeter.

25 **Keywords:**

26 Biomechanics; Insect adhesion; Insect cuticle; biomaterials; Poisson's ratio

27 **1 Introduction**

28 Many insects possess fluid-mediated adhesive pads to safely adhere to almost all
29 known surfaces [1,2]. Whilst the adhesive pads of several insect groups such as flies
30 and beetles are densely covered with flexible setae, the smooth pads found in other
31 insects such as ants, stick insects and cockroaches are “pillow-like” soft structures.
32 Although obviously distinct in their morphology, both designs provide good adhesion
33 to surfaces with unpredictable roughness by maximizing the contact area between the
34 pad and the surface. In smooth adhesive pads a two-phasic adhesive secretion helps to
35 fill gaps between small surface asperities and allows the insects to combine capillary
36 adhesion with resistance against sliding [3].

37 Besides the presence of an adhesive emulsion, an additional remarkable adaptation of
38 the smooth arolia is the highly specialised adhesive cuticle. It is characterized by
39 fibrils which are aligned almost perpendicularly to the surface [4-8]. SEM of freeze
40 fractures and TEM of the arolium of stick insects (*Carausius morosus*) showed that
41 these cuticular rods originate from the endocuticular layer and are 44 to 74 μm long
42 with an average diameter of 1.65 μm . Towards the surface the thick rods branch into
43 finer fibrils [7]. This specialised type of cuticle has evolved several times
44 independently in Arthropods, but its detailed function is still unclear. The branched
45 fibril structure probably helps the pads to conform to surface roughness at different
46 length scales [9,10]. Moreover, it has been proposed that the fibrous structure is
47 responsible for the pads' frictional anisotropy, i.e. the higher friction of pads in the
48 pulling direction, which allows animals to increase adhesion by opposing their feet,
49 thereby achieving shallower force vectors [11,12]. It has been found that this direction
50 dependence is largely explained by the variation in adhesive contact area [1].
51 However, it is still unclear what role the fibrillar ultrastructure plays for this dynamic
52 reaction.

53 A dynamic control of adhesive contact area has been demonstrated for ants that can
54 actively and passively change the size of their contact area [13]. When the legs are
55 pulled towards the body, ant adhesive pads in partial contact with a surface can
56 rapidly unfold. Due to the ‘chain-like’ morphology of the segmented insect tarsus, a
57 distal adhesive pad can transmit significant forces only in the pulling direction, and both
58 pushing forces and lateral forces are likely small. The passive, purely mechanical

59 nature of the ants' unfolding reaction is confirmed by the finding that it can occur
60 extremely fast, sometimes within less than a millisecond [14]. This passive increase of
61 adhesive contact area allows insects to quickly react to mechanical perturbations such
62 as wind or raindrops [13,15]. Neuronally controlled reflexes in insects typically take
63 much longer (>5 ms in the locust leg [16]; 10-15 ms for *Blatta orientalis* and
64 *Periplaneta americana* [17]). This delay clearly excludes a neuromuscular control of
65 the contact area within this time frame [13,16].

66 It is unlikely that such useful mechanical "preflexes" are confined to ants, and
67 preliminary findings indeed indicate that a similar preflex reaction occurs in stick
68 insects (*Carausius morosus*), where the arolium cannot be unfolded, in contrast to the
69 situation in ants and bees [14]. Variation of the direction of the shear movement
70 showed that the passive variation of contact area is direction dependent. As in ants,
71 contact area increased for pulls and decreased for pushes [14].

72 If muscular control cannot explain the increase of contact area, what is the underlying
73 mechanism of these passive reactions? For the smooth pads of ants it has been shown
74 that the complex mechanical arrangement of the arolium results in the passive
75 unfolding of the pad [13]. However, no such morphological adaptation is present in
76 the smooth pads of other insect species, such as stick insects or cockroaches. Could
77 the specialised cuticle of the pads itself play a role in the increase of contact area?

78 If shearing of the cuticle is linked to a change of the fibril orientation, a proximal pull
79 (towards the body) should reduce the fibril angle and decrease the thickness of the
80 adhesive cuticle. Assuming that the cuticle is a cuboid with constant volume (height x
81 width x length), any change of fibril orientation should be correlated with a change of
82 contact area, as the pad is expected to expand along the proximal-distal and the lateral
83 axis when the height decreases. Conversely, a distal pushing movement (away from
84 the body) may lead to an increased fibril angle, resulting in a contraction of the
85 adhesive contact area and easier detachment (see Figure 1).

86 In this study we test this hypothesis by using fluorescence and interference reflexion
87 microscopy to quantify *in vivo* the effect of proximal pulls on the fibril orientation and
88 to measure the strain within the adhesive contact zone.

89 2 Materials and methods

90 2.1 Study animals

91 Adult female Indian stick insects (*C. morosus*) were taken from a laboratory colony in
92 which insects were kept at 24°C and fed with water and food *ad libitum*.

93 Making use of their natural stick-like mimesis posture with their legs in line with the
94 body, the stick insects were slid into a glass Pasteur pipette with their front legs
95 protruding. The tarsus of one leg was fixed to a rigid soldering wire attached to the
96 pipette. The last tarsal segments and the non-adhesive dorsal side of the arolium were
97 carefully embedded in fast-hardening dental cement (Prottemp, ESPE) to prevent any
98 active movements of the adhesive organ (see Figure 1 A).

99 2.2 Visualisation of the fibril structure

100 The arolia of the fixed legs were brought into contact perpendicularly with a smooth
101 glass coverslip (“normal” position) and then carefully pulled over 50 µm in the
102 proximal direction (“pull”) using a micromanipulator (speed approx. 10µm/s)
103 mounted on the microscope stage. Great care was taken to ensure that the adhesive
104 pad remained in static contact with the substrate at all times, as any sliding movement
105 with a resulting shift of the fibril pattern would have interfered with the automated
106 fibril angle measurements.

107 The fibrous cuticle of the adhesive pad shows a characteristic blue auto-fluorescence
108 under UV illumination. This suggests that it contains resilin (although more rigorous
109 tests are required for confirmation), a protein providing high resistance to mechanical
110 fatigue frequently found in regularly deforming cuticle [18,19]. To increase the
111 signal-to-noise ratio and reduce image distortions to a minimum, images were
112 recorded using a mercury short-arc lamp (HBO 103 W/2, Osram) at an excitation
113 wavelength of 365 nm and emission wavelengths of > 425 nm. At this illumination
114 the adhesive fluid within the contact zone did not fluoresce and thus did not interfere
115 with the measurements.

116 A Leica DRM HC microscope equipped with a motorized stage (LSTEP, Märzhäuser)
117 and a triggered camera (10 bit monochrome CCD QICam, INTAS) were used to
118 capture image stacks at 100x magnification and a frame rate of 1 Hz (500ms exposure
119 time + 500ms movement of the stage). These stacks consisted of 100 consecutive

120 images focussing “into” the pad’s cuticle (starting slightly outside the pad), and 100
121 images captured whilst focussing “out”, with a z-distance between consecutive frames
122 of 0.192 μm . For the analysis, we selected 50 consecutive frames from the inwards
123 movement and the 50 corresponding frames from the outwards movement for the
124 automated tracking, starting at approx. 4 μm focal depth. By comparing the "in" and
125 "out" patterns we checked the stacks for pad movements during the capturing process.
126 Throughout the paper, we refer to the optical axis of the microscope (i.e. the axis
127 perpendicular to the glass substrate) as z-axis; the projection of the leg onto the
128 surface (i.e. the direction of the pushing/pulling movement) is called x-axis and the
129 transverse direction (orthogonal to x and z) y-axis (see Fig.1).

130 Measurements of the contact area of the same pads were taken before and after the
131 shear movement at 5 x magnification using reflected light and a custom-made Matlab
132 script.

133 **2.3 Reconstruction of the fibril structure**

134 The human eye is very good at pattern recognition and pattern completion, even at
135 relatively low signal-to-noise ratios [20,21]. While the small individual fibrils were
136 not clearly visible on single images, the movement of the pattern was apparent in
137 animated image stacks (see videos 1 and 2).

138 To eliminate any observer bias, all identification characteristics were removed from
139 the image stacks and the data were analysed in random order. To reduce noise and
140 increase the visibility of the fibrils, each frame was 2D-FFT-bandpass filtered (90 nm-
141 4.5 μm). Fibril angles were manually digitised from sagittal views in the middle of the
142 pad using the ImageJ “volume viewer” plug-in [22] (the sagittal view corresponds to
143 the x-z-plane in Figure 1).

144 Using a different, automated image analysis method, we verified the fibril angle
145 results obtained by digitisation of sagittal views (see videos 1 and 2). The fibril
146 structure's displacement vectors from one image of the z-stack to the next were
147 tracked using an optical flow algorithm [23], developed using the CImg library. As
148 the depth (z-position) of the imaging plane was moved through the cuticle, the local
149 rate of displacement with depth provided a measure of the fibril angle.

150

151 Data for fibril angles and contact area were tested for normal distribution using
152 “Kolmogorov-Smirnov” and paired t-tests were used to test for significant differences
153 between the “normal” and the “pulled” group. If not stated otherwise, all values are
154 given as means \pm standard error (s.e.).

155 **2.4 Direct strain measurements in the contact zone**

156 To analyse the detailed mechanism of contact area increase, we studied the adhesive
157 contact zone of stick insect arolia during pushing and pulling movements using
158 interference reflexion microscopy (at 100x magnification and monochromatic
159 illumination of 546 nm). Stick insects were mounted as before, but on a
160 micromanipulator outside the microscope stage, and the arolium of one foot was
161 brought into contact with a glass coverslip mounted on a holder on the microscope
162 stage. Three pairs of short (50 μm displacement) pulls and pushes were performed by
163 moving the microscope stage, with a velocity of 100 $\mu\text{m s}^{-1}$ and 2 s pause after each
164 movement.

165 Images of different regions of the contact zone were recorded at 2 Hz. To avoid blur
166 during the pad movement, we analyzed the first or second frame after the
167 pulls/pushes. The characteristic pattern of folds in the contact zone allowed us to
168 quantify the strain both along the x and the y axis (i.e. proximal-distal and lateral)
169 caused by the pushing-pulling movements (see Figure 1 A). We define strain for our
170 situation as

$$171 \quad \varepsilon = \frac{l_{pull} - l_{push}}{l_{push}}, \quad (1)$$

172 where l_{pull} and l_{push} are the distances between two characteristic points in the contact
173 zone after a pull or push, respectively.

174 **3 Results**

175 **3.1 Effect of pulling on the fibril angle**

176 The UV fluorescence image stacks of *C. morosus* adhesive pads clearly revealed the
177 three-dimensional, fibrous structure of the procuticle (see Figure 2 B and C).

178 The mean angle measured from reconstructed sagittal views of the fibril structure for
179 the normal pad position was $71.26 \pm 1.3^\circ$ ($n=10$). After the pulling movement the
180 mean angle was significantly reduced to $61.44 \pm 1.3^\circ$ ($n=10$, $t_9=7.43$, $P<0.001$, see
181 Figure 3 A).

182 The angles measured using the automated tracking were consistent with the angles
183 digitized from reconstructed sagittal views. A direct comparison between manual
184 digitisation and automated tracking showed perfect consistency (65.5° vs. 63.2° , see
185 Video 2). However, although the automated tracking method provided reliable
186 measurements for intermediate fibril angles, it could not resolve the smaller angles
187 after proximal pulls. Thus the manual digitization of reconstructed sagittal views
188 proved to be the better option.

189 **3.2 Effect of pulling on the adhesive contact area**

190 The contact areas of the adhesive pad were significantly higher after the pulling
191 movement (paired t-test, $t = -11.40$, $P<0.001$) with a mean of $60144 \mu\text{m}^2$ for the
192 “normal” and a mean of $72504 \mu\text{m}^2$ for the “sheared” condition (see Figure 3 B).
193 Thus, the pull increased the contact area on average by $20.80 \pm 1.72 \%$ ($n=10$).

194 After the pull, the proximal-distal “length” of the contact area (measured along the
195 proximal-distal ‘middle line’ of the contact area) was largely unchanged (paired t-test,
196 $t_9=-0.253$, $P>0.05$), whereas the lateral (transverse) “width” significantly increased
197 (paired t-test, $t_9=12.43$, $P<0.001$). Therefore, the aspect ratio of the contact area (i.e.
198 width/length) significantly increased from 2.70 ± 0.06 to 3.15 ± 0.06 (paired t-test,
199 $t_9=-4.37$, $P<0.001$, see Figure 4). These results show that the increase in contact area
200 was mainly the result of the increased pad width while pad length remained largely
201 constant.

202 The correlation between contact area size and fibril angle was measured by
203 calculating the change in contact area per degree change in fibril angle for each pair
204 of measurements. All ratios were negative and significantly different from zero (mean
205 incline $-1798 \pm 499 \mu\text{m}^2/\text{degree}$, one-sample t-test, $t_9=-3.600$, $P<0.001$).

206 **3.3 Strain in the contact zone**

207 Direct measurements in the adhesive contact zone of stick insects using IRM
208 confirmed the presence of strains (as defined by Equation 1), ranging from -4.0% to

209 8.7%. Strain was positive both in the proximal-distal and in the lateral directions (one-
210 sample t-tests significant both for proximal-distal: $t_{39}=2.92$, $P<0.01$, and lateral:
211 $t_{39}=4.22$, $P<0.001$; Figure 5). However, the relative magnitude of the two in-plane
212 strain components was different depending on the region on the pad. While proximal-
213 distal and lateral strains were not significantly different from each other near the
214 lateral (left and right) edges of the pad ($t_{23}=1.62$, $P>0.1$), the transverse strain
215 dominated significantly in the middle of the contact zone ($t_{14}=3.03$, $P<0.01$, Figure 5).

216 From the overall mean strains of 0.92% (proximal-distal) and 1.87% (transverse), it
217 can be estimated that cuticle expansion during the pull should increase the adhesive
218 contact area by 2.8%. For the pad studied in this experiment, contact area increased
219 from $102445 \pm 1756 \mu\text{m}^2$ (push) to $107919 \pm 1591 \mu\text{m}^2$ (pull), i.e. by 5.3%. Thus,
220 cuticle expansion only partly explains the observed contact area increase.

221 At the same time, the IRM recordings showed that during pulls, new areas of adhesive
222 cuticle came into contact at the edge of the pad. As we could only analyze image pairs
223 where the pad edge was visible both after the pull and the push, our data do not allow
224 a detailed assessment on which sides of the pad contact area was mainly gained (or
225 lost). However, successful image pairs from the distal, lateral edges of the pad contact
226 zone (see Figure 5) show that the "new" cuticle zone added during the pull was as
227 wide as $10.3 \mu\text{m}$ (measured perpendicularly to the pad edge; $n=22$, median= $1.8 \mu\text{m}$,
228 range $0.2 - 10.3 \mu\text{m}$).

229 Assuming that a cuticle zone of $1.8 \mu\text{m}$ width is added around the whole perimeter of
230 the pad (length measured as $1350 \mu\text{m}$), the contact area would grow by $2430 \mu\text{m}^2$, i.e.
231 by 2.4%. This value is in good agreement with the above estimate of 2.8%; the
232 observed contact area increase of 5.3% therefore represents a combination of cuticular
233 expansion (~54%) and addition of new contact area (~46%).

234 3.4 Regular microstructure in the outer arolium cuticle

235 When testing various combinations of surface properties to increase the visibility of
236 the fibril pattern using interference reflection microscopy, we observed a regular
237 "fingerprint" like pattern on the arolia of *C. morosus* (see Figure 6). The pattern
238 consisted of a succession of bright and dark sinusoidal lines oriented transversely, i.e.
239 perpendicular to the distal-proximal axis of the adhesive pad. The mean periodicity of
240 the pattern along the proximal-distal axis was $414.4 \pm 33 \text{ nm}$ ($n=14$).

241 The visibility of this pattern appeared to depend on the refractive index of the
242 substrates. The pattern was visible on Polyimide (PI-2611)-coated coverslips ($n_0 =$
243 1.9) and very clear on mica substrates ($n_0 \approx 1.59$), but it had only weak contrast on
244 glass coverslips ($n_0 = 1.52$). The pattern was present throughout the entire contact
245 area, and it was only visible in the outer zone of the cuticle, up to a focal depth of ca.
246 $2 \mu\text{m}$. Thus, this pattern did not interfere with our fibril angle measurements. The
247 depth of the "fingerprint" pattern suggests that it is the result of a regular, directional
248 arrangement of the fine cuticular fibrils in the outer "branching" zone of the arolium
249 cuticle [7]. Higher-resolution electron microscopy imaging of this zone is required to
250 test this hypothesis.

251 **4 Discussion**

252 Our study shows that *in vivo* measurements and 3D-reconstruction of the fibrils are
253 possible with standard UV fluorescence microscopy. The fibril angles measured using
254 the presented *in vivo* technique varied between 55.19° and 78.62° . These results are in
255 good agreement with 2D SEM images of freeze-fractures of fixed adhesive organs
256 (see Figure 2 A and [7,11]). As the weak UV auto-fluorescence of the cuticle required
257 relatively long exposure times (500ms), our recordings were limited to pads in
258 completely static contact and therefore to small pulling forces. Although insect
259 adhesive pads can generate some static friction [3,24,25] only very small shear forces
260 do not result in any sliding movement over long periods of time. As the friction of
261 insect pads strongly increases with sliding velocity [24] shear forces can be more than
262 ten times larger than this "remaining" friction for faster pulls [3,25]. The fibril angle
263 variation is probably a function of the applied force (acting against spring-like
264 elements tending to return the fibres to their original position). Thus, it is likely that
265 significantly smaller fibril angles will occur for the stronger pulling forces that insects
266 experience under natural conditions. However, studying the fibril angles under such
267 conditions will require methods for statically applying large shear forces to the pad's
268 cuticle.

269 A possible source of error in our fibril angle measurements are image distortions
270 resulting from out-of-focus fluorescence. More advanced microscopic techniques
271 such as confocal microscopy would probably improve the accuracy of the
272 measurements. A better image quality would also facilitate the use of automated

273 image processing algorithms for fibril tracking, which are preferable in terms of
274 speed. Computer-based image deconvolution can effectively reduce noise and
275 increase the image quality of some selected image stacks. However, computation
276 times of 6-8 hours for a single image stack currently restrict the practical use of this
277 method.

278 **4.1 Larger contact areas coincide with smaller fibril angles**

279 Our results show that larger contact areas resulting from pulls coincide with smaller
280 fibril angles. Even very weak pulls significantly increased the contact area and
281 decreased the fibril angle. This confirms the validity of our hypothesis that shearing
282 movements result in changes of the fibril orientation. Can the measured variation
283 explain the observed change in contact area?

284 A simplified model can be used to estimate the effect of the fibrils on the contact area.
285 If the length L of the fibrils is constant, and the cuticle height h is coupled with the
286 fibril angle α ($0^\circ < \alpha < 90^\circ$), the height can be described by

$$287 \quad h = \sin \alpha \cdot L \quad (2)$$

288 Assuming that the volume of the cuticle is constant ($A \cdot h = A' \cdot h'$), where A' and h'
289 denote the contact area and height after a pull, respectively, the new contact area A'
290 should depend on the change of the fibril angle (from α to α') as

$$291 \quad A' = A \cdot \frac{\sin \alpha}{\sin \alpha'} \quad (3)$$

292 So far, no direct experimental support exists for the assumption of constant cuticular
293 volume. However, the assumption is plausible because soft cuticle is a completely
294 water-filled material that does not contain air [26] and water is effectively
295 incompressible at physiological pressures. Thus, a volume change of the cuticle
296 requires fluid flow into or out of this region of the cuticle, which may be slow as it
297 has to pass perpendicularly through the outer membrane of the epidermal cells or
298 laterally through adjacent, relatively thin and dense areas of cuticle. Particularly
299 during rapid pad deformations such as those caused by sudden perturbations, the
300 amount of fluid flow is probably negligible.

301 Equation 3 shows that the observed change of α from 71.26 to 61.44° predicts an
302 increase in contact area of 7.8 %, which is smaller than the observed change of about
303 20 %. This suggests that not only the fibre angle is responsible for the change in
304 adhesive contact area.

305 One possibility is that a pull could slightly rotate the pad, thereby bringing new
306 cuticle area into surface contact on its proximal side. While such a "rolling"
307 movement would have a neutral effect on contact area for a spherical pad, the contact
308 area could increase for other pad shapes such as asymmetrical "bean-like" pads,
309 which have a smaller radius of curvature on the distal than on the proximal side. In
310 this situation, even small changes of the pad's orientation could result in
311 overproportional changes in contact area. A "rotation" model could also explain the
312 observed change of the adhesive contact area's shape.

313 However, the results of our strain measurements in the adhesive contact zone speak
314 against a simple "rotation" model. Firstly, we found that new contact area is also
315 added at the distal margin of the contact zone. Secondly, the observed contact area
316 increase occurred not only by the addition of new contact area at the pad edge but also
317 by expansion of the adhesive cuticle.

318 Therefore, a third, related mechanism may apply, where both pad rotation and
319 reduction of the fibril angle increase the hydrostatic pressure in the cuticle, tending to
320 expand the contact area in all directions.

321 This prediction in turn contrasts with our finding that pulls significantly increased the
322 "width" of the contact area but left the proximal-distal "length" virtually unchanged.
323 The dominance of lateral over proximal-distal expansion was also evident from our
324 strain measurements within the contact area. It therefore appears that despite a
325 tendency to expand in all directions, the adhesive cuticle responds to pulls by
326 elongating only slightly along the pull but strongly in the lateral direction. This
327 behaviour may be based on the cuticle's ultrastructure. Lateral expansion may involve
328 a lateral "fanning out" of the rods. While perfectly perpendicular rods should fan out
329 equally well in the proximal-distal and the lateral directions, proximal-distal fanning
330 may become constrained for smaller rod (fibril) angles so that lateral expansion
331 should dominate. Moreover, the folding pattern in the adhesive contact zone (see

332 Figure 5 A) might also play a role. As these folds run mainly along the proximal-
333 distal axis, the cuticle and epicuticle may be more extensible in the lateral direction.

334 **4.2 A proximal pull leads to a lateral expansion of the contact area**

335 Our results show that the pad cuticle responds to a proximal-distal pull with a lateral
336 expansion. This unusual behaviour suggests that smooth pad cuticle is a material with
337 a negative Poisson's ratio. For a material, the Poisson's ratio is the negative of the ratio
338 of lateral to axial strain under uniaxial extension or compression. Negative Poisson's
339 ratios have been observed for some anisotropic crystals and materials comprised of
340 fibrous networks [27-29].

341 The dynamic control of adhesive contact area investigated here for stick insects is
342 analogous to the passive increase of adhesive contact area in ants [13]. As in ants, a
343 passive, purely mechanical “preflex” reaction may allow insects to respond instantly
344 to perturbations tending to detach them from the substrate. Besides the advantage of a
345 rapid contact area increase for unexpected mechanical perturbations, a change of the
346 fibril angle could also assist a controlled peeling movement of the proximal rim of the
347 contact zone. The stress distribution at the peeling edge is determined by the bending
348 stiffness of the cuticle [30]. Reducing the fibril angle by a pull may result in a smaller
349 proximal-distal distance between the single fibres, likely increasing the bending
350 stiffness of the adhesive pad's cuticle. This would prevent peeling and thereby
351 increase adhesive forces. Conversely, pushing movements may produce more
352 perpendicularly orientated fibrils, making the cuticle more easily deformable and
353 peelable and allowing easy detachment during locomotion.

354 While almost all previous attempts to produce biomimetic adhesives have focused on
355 the gecko's fibrillar adhesive system, the potential of smooth pads as a source of
356 inspiration is still untapped. Fibrous auxetic (negative Poisson ratio) structures might
357 provide a new mechanism for adhesives to achieve rapid attachment and detachment
358 via shear forces [12]. Application of this principle in synthetic adhesive pads may
359 help the development of controllable adhesives and climbing robots.

360 **Acknowledgements**

361 This study was financially supported by fellowships of the German National
362 Academic Foundation, the Irish Research Council for Science, Engineering and
363 Technology (to J.-H.D.), the Biotechnology and Biological Sciences Research
364 Council (BB/E004156/1 to W.F.) and a scholarship from Tongyi University (to M.L.).
365 The SEM image in Figure 2 A was taken by Christofer Clemente.

366

367

368 **References**

- 369 [1] Bullock JMR, Drechsler P, Federle W. Comparison of smooth and hairy
370 attachment pads in insects: friction, adhesion and mechanisms for direction-
371 dependence. *J. Exp. Biol.* 2008;211:3333–3343.
- 372 [2] Dirks JH, Federle W. Fluid-based adhesion in insects - principles and
373 challenges. *Soft Matter* 2011;7: 11047–11053.
- 374 [3] Dirks JH, Clemente CJ, Federle W. Insect tricks: two-phasic foot pad
375 secretion prevents slipping. *J. R. Soc. Interface* 2010;7:587–593.
- 376 [4] Clemente CJ, Dirks JH, Barbero DR, Steiner U, Federle W. Friction ridges in
377 cockroach climbing pads: anisotropy of shear stress measured on transparent,
378 microstructured substrates. *J. Comp. Physiol. A* 2009;195:805–814.
- 379 [5] Kendall MD. The anatomy of the tarsi of *Schistocerca gregaria* Forskal. *Z.*
380 *Zellforsch Mikrosk. Anat.* 1970;109:112–137.
- 381 [6] Roth LM, Willis ER. Tarsal structure and climbing ability of cockroaches. *J.*
382 *Exp. Zool.* 1952;119:483–517.
- 383 [7] Scholz I, Baumgartner W, Federle W. Micromechanics of smooth adhesive
384 organs in stick insects: pads are mechanically anisotropic and softer towards
385 the adhesive surface. *J. Comp. Physiol. A.* 2008;194:373-384.
- 386 [8] Slifer EH. Vulnerable areas on the surface of the tarsus and pretarsus of the
387 grasshopper (Acrididae, Orthoptera) with special reference to the arolium.
388 *Ann. Entomol. Soc. Am.* 1950;43:173–188.
- 389 [9] Beutel RG, Gorb SN. Ultrastructure of attachment specializations of
390 hexapods, (Arthropoda): evolutionary patterns inferred from a revised ordinal

- 391 phylogeny. *J. Zool. Syst. Evol. Res.* 2001;39:177–207.
- 392 [10] Gorb SN. Smooth attachment devices in insects: functional morphology and
393 biomechanics. *Adv. Insect Physiol.* 2007;34:81-115.
- 394 [11] Gorb SN, Scherge M. Biological microtribology: anisotropy in frictional
395 forces of Orthopteran attachment pads reflects the ultrastructure of a highly
396 deformable material. *Proc. R. Soc. Lond. B* 2000;267:1239–1244.
- 397 [12] Autumn K, Dittmore A, Santos D, Spenko M, Cutkosky M. Frictional
398 adhesion: a new angle on gecko attachment. *J. Exp. Biol.* 2006;209:3569-3579
- 399 [13] Federle W, Brainerd EL, McMahon TA, Hölldobler B. Biomechanics of the
400 movable pretarsal adhesive organ in ants and bees. *Proc. Nat. Acad. Sci.*
401 *USA.* 2001;98:6215–6220.
- 402 [14] Endlein T, Federle W. Ants can't be knocked off: A 'preflex' as an extremely
403 rapid attachment reaction. *Comp. Biochem. Phys. A* 2009; S138.
- 404 [15] Federle W, Endlein T. Locomotion and adhesion: dynamic control of
405 adhesive surface contact in ants. *Arthropod Struct. Dev.* 2004;33: 67–75.
- 406 [16] Höltje M, Hustert R. Rapid mechano-sensory pathways code leg impact and
407 elicit very rapid reflexes in insects. *J. Exp. Biol.* 2003;206: 2715–2724.
- 408 [17] Wilson DM. Proprioceptive leg reflexes in cockroaches. *J. Exp. Biol.*
409 1965;43:397–409.
- 410 [18] Andersen SO, Weis-Fogh I. Resilin: a rubber-like protein in arthropodal
411 cuticle. *Adv. Insect Physiol.* 1964;2:1–65.
- 412 [19] Burrows M, Shaw SR, Sutton GP. Resilin and chitinous cuticle form a
413 composite structure for energy storage in jumping by frog hopper insects.
414 *BMC Biology* 2008;6:41.
- 415 [20] Fahle M. Human pattern recognition: parallel processing and perceptual
416 learning. *Perception* 1994;23:411–427.
- 417 [21] Sutherland NS. Outlines of a theory of visual pattern recognition in animals
418 and man. *Proc. R. Soc. Lond. B* 1968;171:297–317.
- 419 [22] Abramoff MD, Magelhaes PJ, Ram SJ. Image processing with ImageJ.
420 *Biophotonics International.* 2004;11:36–42.
- 421 [23] Beauchemin SS, Barron JL. The computation of optical flow. *ACM Comput.*
422 *Surv.* 1995;27:434–466.
- 423 [24] Federle W, Baumgartner W, Hölldobler B. Biomechanics of ant adhesive

- 424 pads: frictional forces are rate- and temperature-dependent. *J. Exp. Biol.*
425 2004; 207:67–74.
- 426 [25] Drechsler P, Federle W. Biomechanics of smooth adhesive pads in insects:
427 influence of tarsal secretion on attachment performance. *J. Comp. Physiol. A*
428 2006;192:1213–1222.
- 429 [26] Neville AC. *Biology of the arthropod cuticle*. Berlin: Springer (1975).
- 430 [27] Evans KE. Tensile network microstructures exhibiting negative Poisson's
431 ratios. *J. Phys. D* 1989;22:1870–1876.
- 432 [28] Burke M. A stretch of the imagination. *New Scientist* 1997;154: 36–39.
- 433 [29] Lakes RS. Foam structures with a negative Poisson's ratio. *Science*
434 1987;235:1038–1040.
- 435 [30] Kaelble DH. Theory and analysis of peel adhesion: bond stresses and
436 distributions. *J. Rheol.* 1960;4:45–73.
- 437

438

439 **Figure 1:** Hypothetical model for the passive contact area increase of smooth pads. A)
 440 Schematic drawing indicating the orientation of the fibrils within a fixed adhesive pad
 441 and the orientation of the axes used in this study. The lateral y-axis is orientated
 442 perpendicular to the image plane. B) A pulling movement of the pad on the surface
 443 may reduce the angle α of the cuticular fibres. Assuming a constant length of the
 444 fibrils, reducing the fibril angle will reduce the structure's height (h). If the structure's
 445 height decreases, the average spacing between the fibres ds (measured within the x-z-
 446 plane) will be reduced, too. This "compression" might increase the effective elastic
 447 modulus of the adhesive pad. C) If the volume of the fibrous structure is constant ($a \times$
 448 $b \times h$), decreasing its height to h' should enlarge the contact area by a factor of h/h' .

449 **Figure 2:** A) SEM image of a freeze fractured *C. morosus* arolium showing the
 450 branching fibrils within the outer cuticle layer. B) Reconstructed fibril structure from
 451 UV fluorescence image stacks of an adhesive pad in "normal" contact (*C. morosus*,
 452 contact area at top). C) After a proximal pull the angle of the fibres to the cuticle
 453 surface decreased.

454 **Video 1:** Field images illustrating the results of automated tracking of a fibrous
 455 structure in the contact zone from *C. morosus* from selected frames over a focal depth
 456 of 9.7 μm . The arrows show the primary vector length and orientation for each point
 457 of the frame's analysis grid (proximal-distal from left to right). The depth indicated is
 458 measured from the contact area.

459 **Video 2:** Automatically reconstructed apparent fibril "movement" of 4.9 μm over a
 460 focal depth of 9.7 μm for the image sequence of video 1, resulting in a fibril angle of
 461 63.2°. The square represents the tracked movement of the whole pattern.

462 **Figure 3:** A) Fibril angles of one adhesive pad (*C. morosus*) before and after a
 463 proximal pull of 50 μm . The two groups are significantly different (paired t-test,
 464 $t_9=7.43$, $P<0.001$). B) After the pull the contact areas of the adhesive pad were
 465 significantly larger (paired t-test, $t_9=-11.40$, $P<0.001$).

466 **Figure 4:** Change in contact area proportions of *C. morosus* after a proximal pull of
 467 ca. 50 μm . A) Whilst the proximal-distal "length" of the adhesive pads did not

468 significantly increase after a pull, the lateral “width” did (for details see text). B) After
469 the pull the aspect ratio (width/length) of the contact area increased significantly.

470 **Figure 5:** Strain measurements in the adhesive contact zone of *C. morosus*. A)
471 Interference reflexion microscopy images of corresponding area of the contact zone
472 after a push (left) and a pull (right). Lines mark length measurements between
473 corresponding landmarks on the pad to calculate proximal-distal and lateral strain. B)
474 Summary of proximal-distal and lateral strain measurements at different positions of
475 the pad (left, middle and right region of the contact area). See text for the definition of
476 pulling strain.

477 **Figure 6:** A) Interference reflexion microscopy image of *C. morosus* arolium in
478 contact with a mica surface (illuminating numerical aperture: 0.27, $\lambda=546$ nm,
479 brightness and contrast enhanced). B) Fourier filtering of the image reveals a regular,
480 fingerprint-like micro-pattern with a proximal-distal periodicity of 414.4 ± 33 nm
481 (mean \pm s.e., n=14). The proximal part of the arolium is on the right side of the
482 images.

483

Figure 1

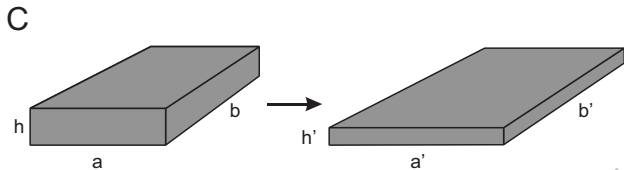
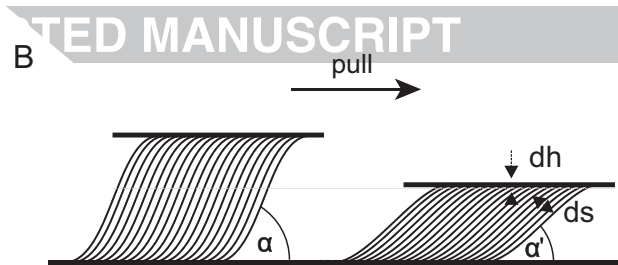
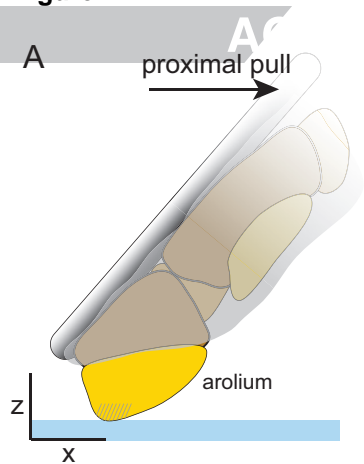


Figure 2

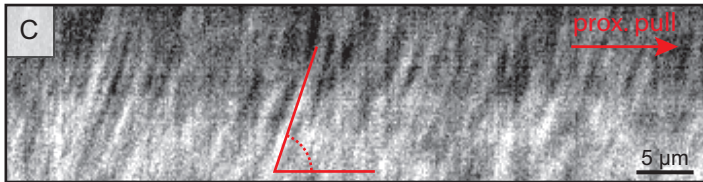
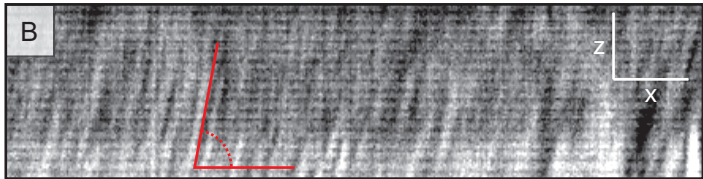
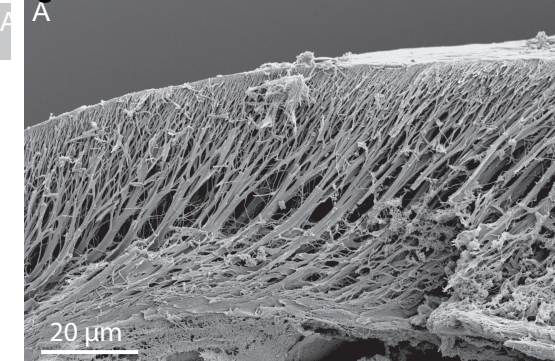


Figure 3

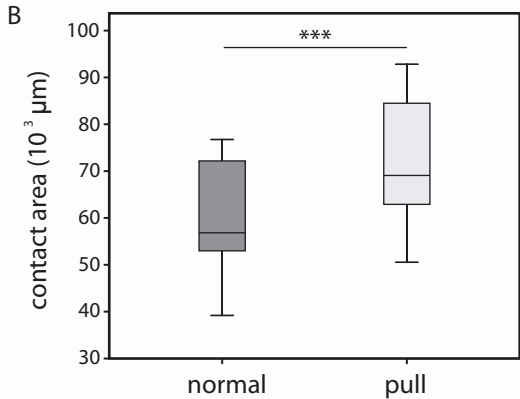
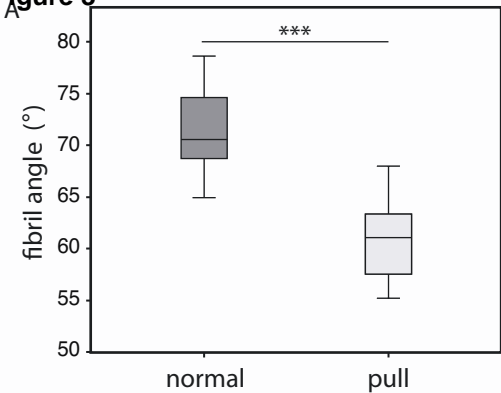


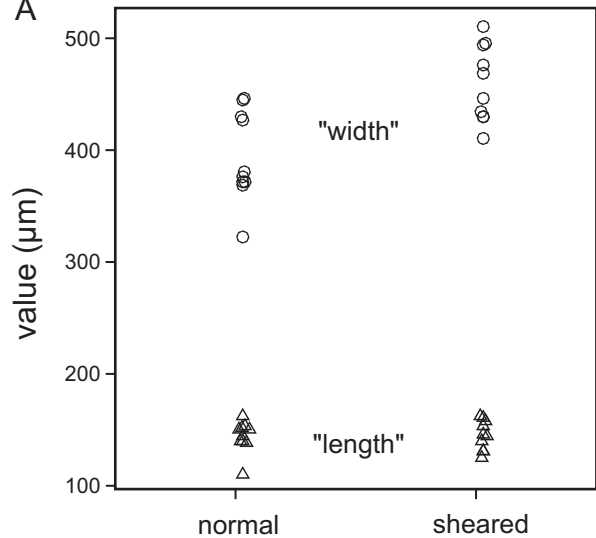
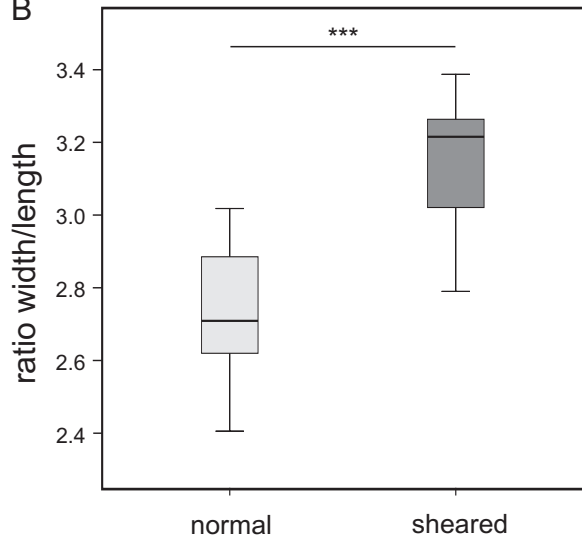
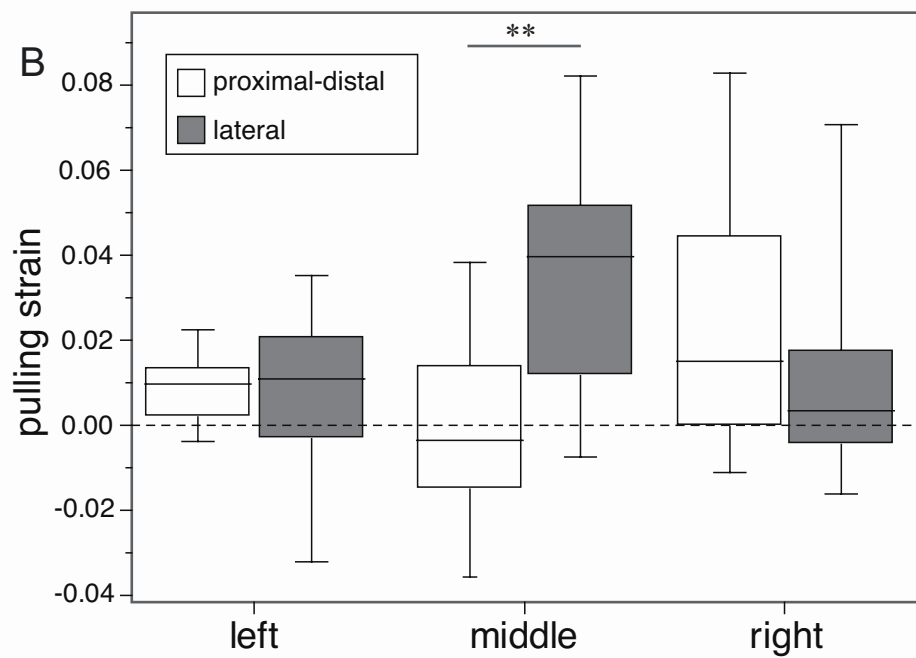
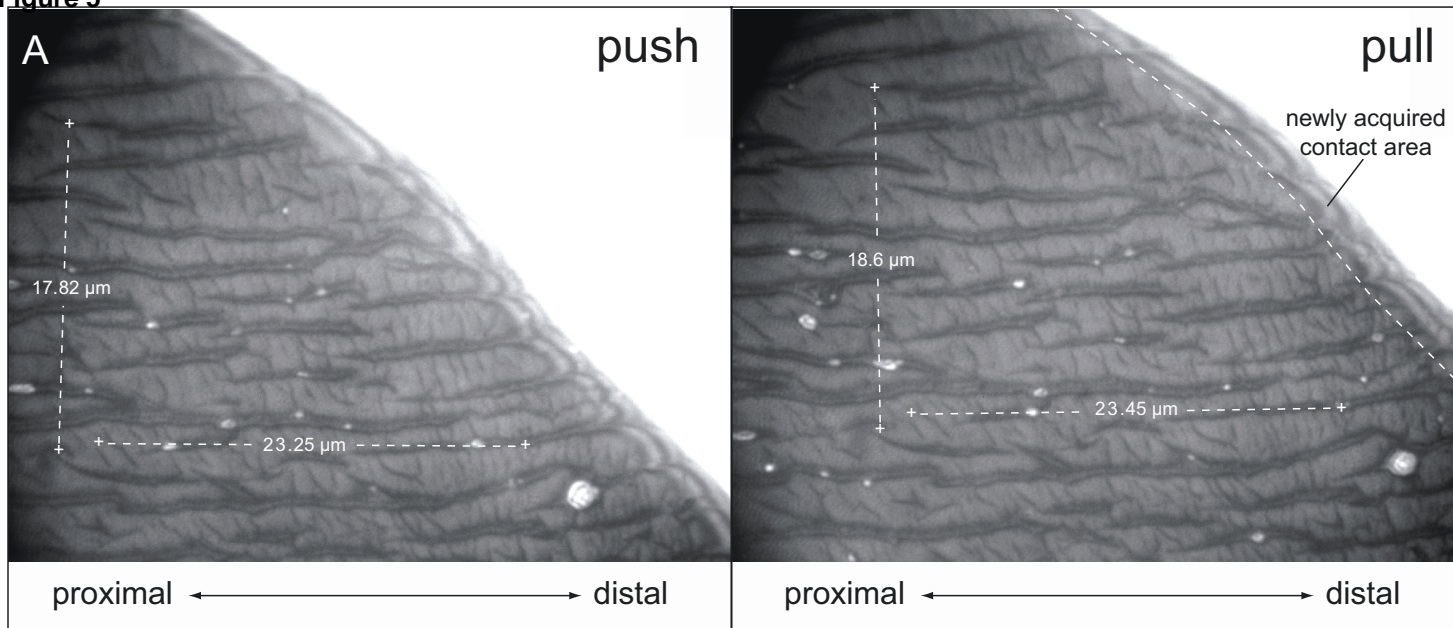
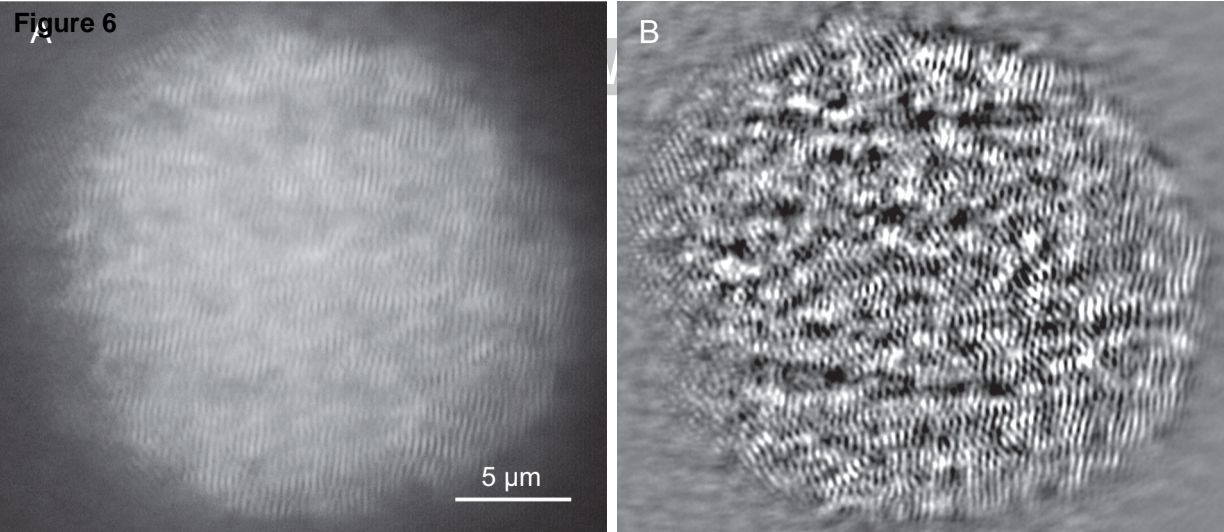
Figure 4**A****B**

Figure 5





Smooth adhesive pad

proximal pull increases contact area

ACCEPTED MANUSCRIPT

